Journal of Biomechanics 110 (2020) 109956

Contents lists available at ScienceDirect

Journal of Biomechanics

journal homepage: www.elsevier.com/locate/jbiomech
www.JBiomech.com

Mechanics of human vocal folds layers during finite strains in tension, compression and shear

Thibaud Cochereau [a,b], Lucie Bailly [a,*], Laurent Orgéas [a], Nathalie Henrich Bernardoni [b], Yohann Robert [c], Maxime Terrien [d]

[a] Univ. Grenoble Alpes, CNRS, Grenoble INP, 3SR, 38000 Grenoble, France
[b] Univ. Grenoble Alpes, CNRS, Grenoble INP, GIPSA-lab, 38000 Grenoble, France
[c] Univ. Grenoble Alpes, CHU Grenoble Alpes, LADAF, 38000 Grenoble, France
[d] Univ. Grenoble Alpes, CNRS, Grenoble INP, LGP2, 38000 Grenoble, France

ARTICLE INFO

Article history:
Accepted 14 July 2020

Keywords:
Vocal folds
Mechanical tests
Tension
Shear
Compression

ABSTRACT

During phonation, human vocal fold tissues are subjected to combined tension, compression and shear loading modes from small to large finite strains. Their mechanical behaviour is however still not well understood. Herein, we complete the existing mechanical database of these soft tissues, by characterising, for the first time, the cyclic and finite strains behaviour of the *lamina propria* and *vocalis* layers under these loading modes. To minimise the inter or intra-individual variability, particular attention was paid to subject each tissue sample successively to the three loadings. A non-linear mechanical behaviour is observed for all loading modes: a J-shape strain stiffening in longitudinal tension and transverse compression, albeit far less pronounced in shear, stress accommodation and stress hysteresis whatever the loading mode. In addition, recorded stress levels during longitudinal tension are much higher for the *lamina propria* than for the *vocalis*. Conversely, the responses of the *lamina propria* and the *vocalis* in transverse compression as well as transverse and longitudinal shears are of the same orders of magnitude. We also highlight the strain rate sensitivity of the tissues, as well as their anisotropic properties.

1. Introduction

Human vocal folds are anisotropic soft tissues, comprising two principal layers: the *lamina propria*, *i.e.*, a loose connective tissue made of collagen and elastin fibers, and the *vocalis*, composed of skeletal "muscle fibers" (Fig.1; Hirano, 1974). The fiber arrangement within these layers exhibits a pronounced alignment along the antero-posterior (or longitudinal) direction $\mathbf{e}_z$ of the vocal folds (Fig.1; Hirano, 1974; Miri et al., 2013). During phonation, vocal folds are deformed due to pulmonary airflow and laryngeal motions, enduring vibrations of various amplitudes, frequencies, and degrees of collision. These multiple configurations imply complex and coupled multi-axial mechanical loadings experienced by the tissue upon finite strains and at various strain rates. These loadings include combined longitudinal tension and compression which are mainly due to laryngeal muscular contractions along $\mathbf{e}_z$ (Fig. 1), but also transverse compression due to aerodynamic forces and vocal-fold collision along $\mathbf{e}_x$, as well as longitudinal and transverse shears due to oscillatory motion along $\mathbf{e}_y$ and friction stresses between both vocal folds (Miri, 2014). These observations are confirmed with finite element simulations of vocal folds oscillations during phonation (Gunter, 2003, 2004; Vampola et al., 2016; Vampola and Horáček, 2014; Tao and Jiang, 2007), bringing fruitful semi-quantitative information. However, current simulations suffer from a lack of experimental data, to use more relevant constitutive mechanical models of vocal tissues.

To investigate the mechanics of vocal-fold tissues, several experimental works have been conducted during the last twenty years (Goodyer et al., 2011; Miri, 2014; Dion et al., 2016). Most of them focused on the *lamina propria* response during longitudinal tension. They highlighted the non-linear behaviour of this tissue showing a J-shape stress–strain curve upon loading, and thus, an increasing tangent longitudinal modulus E_z^t from 10 kPa to 2000 kPa (Kelleher et al., 2011; Kelleher et al., 2013b; Chan et al., 2007; Min et al., 1995; Kelleher et al., 2010). Viscoelastic properties of this layer were also investigated using either standard shear Dynamic Mechanical Analysis (DMA), *i.e.*, within the linear regime (Chan and Titze, 1999; Chan and Rodriguez, 2008; Goodyer et al., 2006; Rohlfs et al., 2013), or more recently using Large Amplitude

* Corresponding author.
E-mail address: lucie.bailly@3sr-grenoble.fr (L. Bailly).

https://doi.org/10.1016/j.jbiomech.2020.109956
0021-9290/

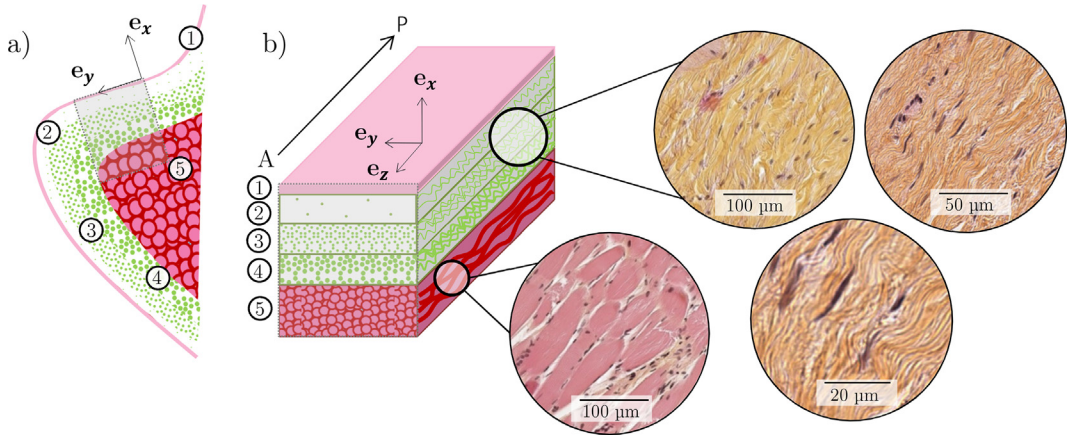

Fig. 1. Human vocal-fold histology. (a) Mid-coronal view of one fold in the larynx: idealised scheme; (b) *(left)* Zoom on the fold sublayers and fibrous microstructure: ① *Epithelium*, ②+③+④ *Lamina propria*, ⑤ *Vocalis* muscle. *Lamina propria* sublayers: ② superficial, ③ intermediate, ④ deep. *(right)* Corresponding 2D histological photomicrographs of L_3–LP_2, L_4–LP_2, L_3–M_2 and L_4–LP_2 (*from top to bottom, left to right*), prepared with HES stain: collagen fibers (yellow orange); cytoplasms, striated muscular and elastin fibers (pink); *nuclei* (blue-purple). (For interpretation of the references to colour in this figure legend, the reader is referred to the web version of this article.)

Oscillatory Shear (LAOS) (Chan, 2018). These works allowed to characterise the shear storage G' and loss G'' moduli (DMA) of the *lamina propria*, as well as its cyclic and finite strains shear behaviour (LAOS) within the (x,y) plane. Several conclusions can be drawn therefrom. Firstly, G' and G'' (i) are of the same order of magnitude and exhibit a non-linear shear rate stiffening, (ii) vary within a wide range of values (from 1 Pa to 10 kPa), that are much lower than those recorded for E_z^t. Point (i) proves that viscous effects play a key role on the mechanics of the *lamina propria*. Point (ii) emphasises the anisotropy of the *lamina propria* behaviour, which is directly induced by its structural anisotropy (Bailly et al., 2018). Secondly, the *lamina propria* cyclic shear stress–strain curves also exhibited a J-shape, with an increase of the strain stiffening above a shear strain around 0.5 (Chan, 2018).

Despite this important database, there are still some issues to be tackled to understand and model the mechanics of human vocal folds. Among them is the difficulty to analyse experimental results due to the large variability of the mechanical response between subjects, and within the tissues themselves (Chan et al., 2007; Chan and Titze, 1999; Rohlfs et al., 2013), as for other soft living materials (Cavinato et al., 2019). It is thus challenging to compare data obtained with different mechanical loadings, *e.g.*, tension and shear. In addition, the mechanics of the *lamina propria* during transverse compression has never been studied so far. This constitutes a crucial lack in current knowledge, keeping in mind that the quality of contact between vocal folds is a key factor in voice quality, and that high-impact transverse compressive stresses are believed to generate common lesions in the *lamina propria* after a phonotrauma (Hantzakos et al., 2009; Lagier, 2016). Finally, the mechanics of the *vocalis* has been often discarded up to now, although being a major vocal-fold sublayer used to tune the phonation process, in its active but also passive state.

Therefore, this study aims to provide a new mechanical dataset of human vocal-fold tissues, subjected to a series of physiological loadings, *i.e.,* longitudinal tension, transverse compression as well as longitudinal and transverse shear. These testing conditions were achieved sequentially on each sample, thereby minimising inter-sample variability. We studied and compared the finite strains mechanical responses of both upper layers, including *epithelium* and *lamina propria* (Fig. 1), to those of the *vocalis* muscle for each loading mode. Finally, we quantified the strain rate sensitivity of these tissues, as well as their mechanical anisotropy.

2. Materials and methods

2.1. Vocal folds

Experiments were carried out with 4 healthy human larynges, noted $L_i, i \in [1,2,3,4]$, excised from donated bodies (Table 1) within 48 h *post-mortem*. Procedures were conducted following the French ethical and safety laws related to Body Donation. All but one larynx (*fresh* larynx L_2) were preserved by freezing (-20 °C). Before any manipulation, each frozen sample was slowly thawed for 30 min in tepid water ($T \approx 20$ °C). Vocal folds were then dissected from each laryngeal specimen with portion of thyroid and arytenoid cartilages. Excised vocal folds can be approximated as parallelepiped beams owning a sandwich lamellar structure, oriented along the longitudinal (antero-posterior) direction $\mathbf{e}_z$, as schemed in Fig. 1(b), and pictured in Supplementary Figs. S1(a) and S2(a): they were made of all sublayers from their *epithelium* to the *vocalis* (Fig. 1), and noted L_i-F_j ($j = 1$ and $j = 2$ standing for left and right vocal folds of larynx L_i, respectively). Finally, samples L_3-F_1 and L_4-F_1 were cut in half along the plane $(\mathbf{e}_x, \mathbf{e}_z)$, as shown in Supplementary Fig. S2(b). One half was dedicated to histological analyses, following the protocol detailed in Bailly et al. (2018). The second half was dedicated to mechanical testing.

2.2. Experimental protocol

We designed a protocol to characterise the finite strains mechanics of the *vocalis* and upper layers (*lamina propria* + *epithelium*) under tension, compression and shear, while minimising the inter and intra-individual variability.

2.2.1. Hygro-mechanical set-up

Mechanical tests were conducted at proper hygrometric conditions to prevent the tissues from air drying (Nicolle and Palierne,

Table 1
Origin of the tested larynges.

Larynx name	Gender	Age [y]	Height [m]	Weight [kg]
L_1	Female	78	1.40	40
L_2	Male	80	1.55	50
L_3	Male	79	1.70	65
L_4	Female	79	1.60	45

2010), using a chamber (Fig. 2(a)) in which a saturated air flow ($\approx 95-100\,\%$ RH) was regulated with a humidifier (Fisher and Paykel HC150). We also used a tension–compression micro-press inserted inside the chamber and designed for soft samples (load cell 5 N, relative displacement between crossheads measured with a LVDT sensor) (Latil et al., 2011; Isaksson et al., 2012; Laurencin et al., 2016; Krasnoshlyk et al., 2018; Bailly et al., 2018). For simple tensile tests, specially designed knurled clamps (26 mm width, 7 mm height) were used to facilitate the sample positioning and restrain its slippage (Fig. 2(b)). For simple compression tests, compression platens were hydrated by a film of Phosphate-buffered saline solution, avoiding friction (Fig. 2(b)). For simple shear tests, plates (10 mm length and width) were coated with sand paper to restrain sample slippage (Fig. 2(b)).

2.2.2. Testing protocol

- Tensile tests were first carried out with vocal folds L_i-F_j (Fig. 2 (b)), the gauge length ℓ_0 and cross-section S_0 of which are reported in Table 2. Tests were performed along $\mathbf{e}_z$, *i.e.*, the main fiber orientation. The cell force f signal and the LVDT displacement δ were used to estimate the first Piola-Kirchoff stress $P_{zz} = f/S_0$, as well as the Hencky tensile strain $\varepsilon_{zz} = \ln(1+\delta/\ell_0)$. Each sample was subjected to 10 load-unload cycles at a strain rate $|\dot{\varepsilon}_{zz}| = |\dot{\delta}/\ell_0| \approx 10^{-3}\ \mathrm{s}^{-1}$, up to a moderate tensile strain $\varepsilon_{zz}^{max} = 0.1$ to restrain sample damage.
- Samples were then unmounted, and their upper layers (further labelled L_i-LP_j) were separated from the *vocalis* (L_i-M_j). *Epithelium* was left intact as a remaining part of the L_i-LP_j layer. Care was taken to preserve cartilages parts on both layers. Then, each sample was again subjected to tension loading along $\mathbf{e}_z$ following the aforementioned procedure (see Table 2 for their dimensions).
- Therewith, samples L_i-LP_j and L_i-M_j ($i = 3, 4$) were released from their cartilaginous ends and resized in smaller parallelepiped samples in order to fit compression and shear plates, as described in Fig. S2(c) (see Table 2, "compression" column for their adjusted dimensions). They were then subjected to compression along $\mathbf{e}_x$ (Fig. 2(b)). During the tests, compression stress $P_{xx} = f/S_0$ and compression strain $\varepsilon_{xx} = \ln(1+\delta/\ell_0)$ were recorded. Samples were subjected to 10 load-unload cycles up to $\varepsilon_{xx}^{min} = -0.2$. This procedure was carried out at two strain rates, $|\dot{\varepsilon}_{xx}| = |\dot{\delta}/\ell_0| \approx 10^{-3}\ \mathrm{s}^{-1}$ and $10^{-2}\ \mathrm{s}^{-1}$, respectively.
- Finally, we conducted two consecutive shear tests with the same samples along two different directions, "longitudinal" plane ($\mathbf{e}_z, \mathbf{e}_x$) and "transversal" plane ($\mathbf{e}_y, \mathbf{e}_x$), respectively. During the tests, shear stress $P_{zx} = f/S_0$ (resp. $P_{yx} = f/S_0$) was measured as a function of shear strain $\gamma_{zx} = \delta/\ell_0$ (resp. $\gamma_{yx} = \delta/\ell_0$),

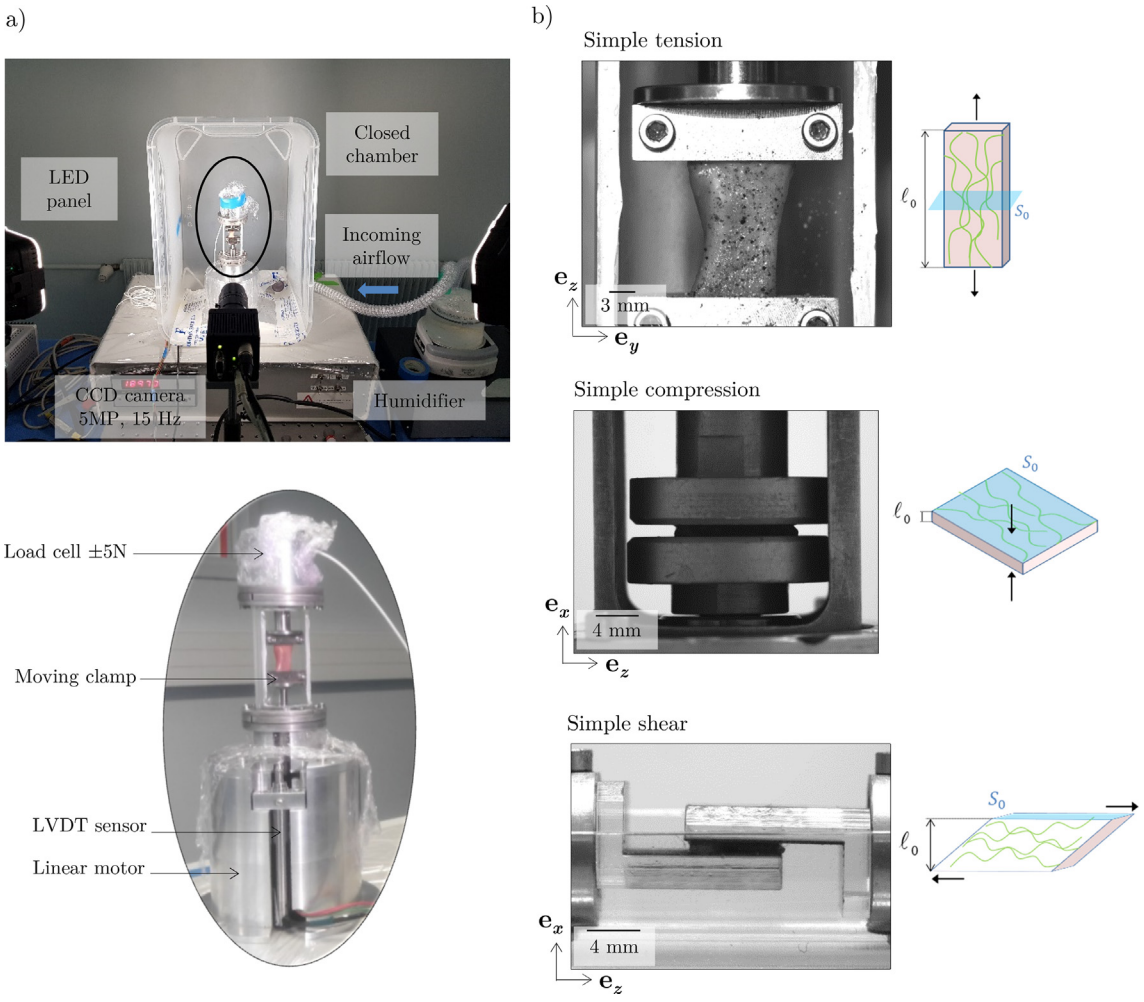

Fig. 2. (a) Overview of the experimental set-up (*top*) and zoom on the uniaxial tension–compression micro-press (*bottom*). (b) Pictures showing the samples when positioned in the micropress for simple tension (*up*), simple compression (*middle*) and simple shear (*down*); the schemes plotted beside of the picture illustrate the main fiber orientation of the samples and their initial dimensions.

Table 2
Sample dimensions used to determine stresses and strains. ℓ_0 is the initial distance between platens or clamps (Fig. 2(b)). The mean initial cross section S_0 and its standard deviation were estimated optically from the width and the thickness profiles of the samples once put onto a flat surface.

	Sample gauge dimensions					
	Tension		Compression		Shear	
Name	ℓ_0 (mm)	$S_0^\dagger$ (mm^2)	ℓ_0 (mm)	$S_0^\dagger$ (mm^2)	ℓ_0 (mm)	$S_0^\dagger$ (mm^2)
L_1–F_1	10.1	28.9 ± 2.4	–	–	–	–
L_1–LP_1	15	8.9 ± 4.8	–	–	–	–
L_1–M_1	7	9.8 ± 4.2	–	–	–	–
L_1–F_2	10.3	40.8 ± 6.1	–	–	–	–
L_1–LP_2	8.5	5.4 ± 3.6	–	–	–	–
L_1–M_2	7.2	14.4 ± 5.8	–	–	–	–
L_2–F_1	16.8	49.2 ± 7.2	–	–	–	–
L_2–LP_1	18	21.3 ± 7.6	–	–	–	–
L_2–M_1	17.8	24.3 ± 9.8	–	–	–	–
L_2–F_2	19.8	38.6 ± 7.2	–	–	–	–
L_2–LP_2	22.3	13.2 ± 7.1	–	–	–	–
L_2–M_2	18.3	19.9 ± 9.3	–	–	–	–
L_3–F_1	14.2	39.0 ± 11.5	–	–	–	–
L_3–LP_1	10	7.4 ± 2.9	1.5	80.0 ± 0.7	1.0	68.5 ± 4.7
L_3–M_1	10	8.8 ± 4.4	1.9	91.9 ± 0.8	1.3	99.0 ± 9.5
L_3–F_2	17.8	82.3 ± 20.2	–	–	–	–
L_3–LP_2	15.7	14.7 ± 4.7	1.1	74.9 ± 5.8	0.9	78.9 ± 0.6
L_3–M_2	11.5	29.3 ± 10.1	2.6	120.1 ± 15.8	2.1	78.0 ± 7.1
L_4–LP_1	15.2	5.8 ± 4.5	0.9	44.8 ± 1.6	0.6	44.6 ± 4.1
L_4–M_1	15.7	11.9 ± 4.0	1.5	81.7 ± 1.2	1.0	84.4 ± 0.3
L_4–LP_2	14	11.7 ± 5.4	1.3	88.6 ± 0.7	1.3	99.0 ± 9.5
L_4–M_2	15.3	14.4 ± 5.6	2.2	93.7 ± 0.9	2.1	72.9 ± 11.9

while subjecting samples to 10 load-unload cycles up to $\gamma_{zx}^{max} = 0.6$ (resp. $\gamma_{yx}^{max} = 0.6$) at a shear rate $|\dot{\gamma}| = |\dot{\delta}/\ell_0| \approx 10^{-3}$ s^{-1}.

3. Results

3.1. General trends in tension

Tensile responses of the vocal folds and their sublayers along $\mathbf{e}_z$ are reported in Fig. 3 for the first cycle, together with the evolution of the longitudinal tangent moduli $E_z^t = \mathrm{d}P_{zz}/\mathrm{d}\varepsilon_{zz}$ with ε_{zz} (for the first loading only).

Variability – Fig. 3 first emphasises a large scattering of the mechanical responses. For instance, at $\varepsilon_{zz} \approx 0.09$, the ratio of maximal and minimal stresses registered in the case of the L_i-F_j samples rises up to 5. This well-known inter-individual variability is ascribed to tissue histological singularities of each donor, which depends on age, gender, tobacco smoking profile (Chan and Titze, 1999; Chan and Titze, 2003; Chan et al., 2007). Conversely, note that the intra-individual variability is much less marked: the ratio of maximal to minimal stresses at $\varepsilon_{zz} \approx 0.09$ is only 1.3 for left and right vocal-fold samples. Similar conclusions are drawn for upper layers L_i-LP_j and *vocalis* L_i-M_j.

Shape of stress–strain curves and corresponding stiffness – Whatever the sample, stress–strain curves exhibit non-linear responses with a J-shape strain-hardening (Fig. 3, *left)* and a strain hardening of tangent moduli (*right*). These trends are related to the recruitment and reorientation of wavy fibers during tension (Min et al., 1995; Gasser et al., 2006; Fratzl et al., 1998). They are less marked for *vocalis* samples, the muscle fibers being straighter than the collagen/elastin fibers of the upper layers at rest (Fig. 1; Bailly et al., 2018). In addition, reported stress–strain curves exhibit stress hysteresis with a non-negligible residual strain after unloading, which may be ascribed to viscoelastic effects together with structure rearrangements.

Comparison between sublayers – Fig. 3 also proves that stress levels in upper layers are much higher than those recorded for the *vocalis*. For example, at ε_{zz} = 0.1, nominal stresses P_{zz} vary from 14 to 50 kPa, from 8 kPa to more than 100 kPa, and from 0.5 kPa to 28 kPa for vocal folds, upper layers, and *vocalis* samples, respectively. A similar conclusion is drawn for the tangent moduli E_z^t (Fig. 3).

3.2. Mechanics in tension, compression and shear for single samples

To get rid of the aforementioned inter or intra-individual variability, focus is now made on samples L_3-LP_2, L_4-LP_2, L_3-M_2 and L_4-M_2, subjected to the protocol purposely designed. Despite this procedure, some stress scatterings remain due to sample dimensions (Table 2): in Figs. 4 and 5 presented hereafter, they have been highlighted with gray corridors surrounding nominal values of stresses. The first figure gives stress–strain curves after subjecting samples L_3-LP_2 and L_3-M_2 to 10 load-unload cycles in tension, compression and shear. The second one reports similar data for samples L_4-LP_2 and L_4-M_2.

Shape of stress–strain curves – Compared to tension along $\mathbf{e}_z$, the compression along $\mathbf{e}_x$ yields to similar J-shape stress–strain curves during the first loading. However, during unloading, compression stress–strain curves exhibit a marked hysteresis with higher residual strains. In addition, stress levels of upper layers are of the same order of magnitude than those of the *vocalis*, which is also different to what is observed in tension. By contrast, stress–strain curves obtained in shear do not exhibit a J-shape, but a practically constant strain hardening. Note that the apparent strain softening produced at the end of the load (notably for the *vocalis*) is probably due to experimental artifacts, such as sample rocking. In addition, despite a slightly stiffer response for the *vocalis* compared to the upper layers, orders of magnitude of stress levels generated within both sublayers are comparable up to 0.2 shear strain. Lastly, the shear stress hysteresis as well as the residual shear strain are limited.

Effect of cycling – Whatever the samples, repeating load-unload sequences yields to progressive (i) decrease of maximal stresses, (ii) decrease of the stress hysteresis, (iii) increase of the residual strains. These evolutions are commonly observed while cycling

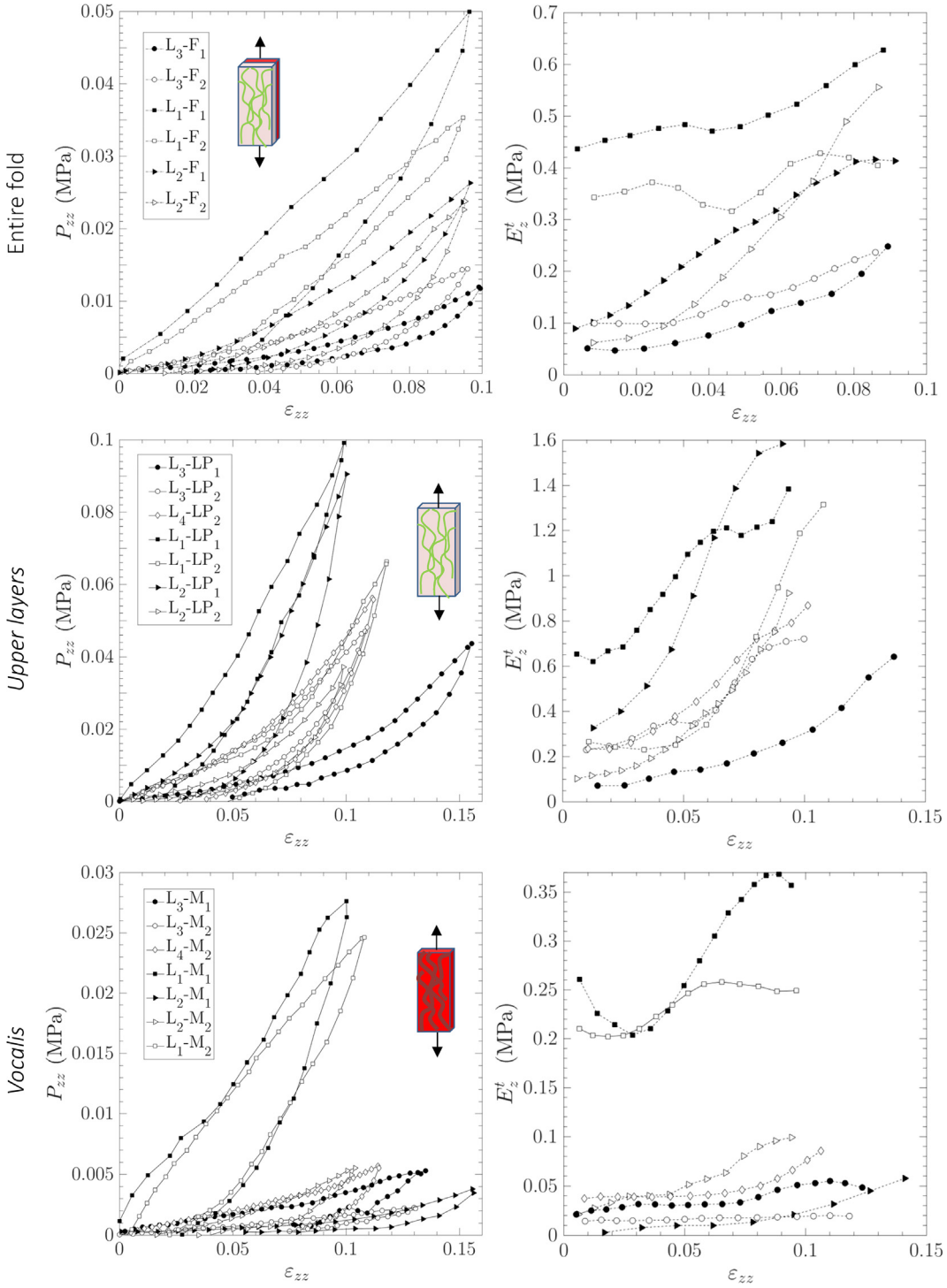

Fig. 3. Tensile behaviour of the vocal folds (*top*), their upper layers (*middle*) and their vocalis (*bottom*) along the sample antero-posterior direction: stress–strain curves (*left*) and corresponding longitudinal tangent modulus E_z^t as a function of ε_{zz} (during the first loading).

soft tissues (Remache et al., 2018) and consistent with previous studies (Zhang et al., 2009; Kelleher et al., 2013; Chan et al., 2007). For both sublayers, these effects are limited in shear (Figs. 4 and 5), but pronounced in tension and compression.

Effect of strain rate – Fig. 6(a) shows typical stress–strain curves obtained with sample L_4-LP_2 compressed at $|\dot{\varepsilon}_{xx}| \approx 10^{-3}$ s^{-1} and $|\dot{\varepsilon}_{xx}| \approx 10^{-2}$ s^{-1}. As expected, the tissue viscoelasticity yields to a moderate to strong increase of stress levels and hysteresis with the strain rate. Fig. 6(b) displays the compression stress ratio P_{xx}^2/P_{xx}^1 of the 8 tested samples with the compression strain during the first loading, where P_{xx}^1 (resp. P_{xx}^2) is the stress at 10^{-3} s^{-1} (resp. 10^{-2} s^{-1}): this ratio ranges within 1.1 and 3.3. For most of samples, it exhibits a slight increase during compression. Furthermore, for the same vocal fold (at fixed i and j-values), the ratios of samples L_i–LP_j and L_i–M_j follow roughly close evolutions.

Anisotropy – The stress–strain response of sample L_3-LP_1 in shear parallel to the $(\mathbf{e}_y, \mathbf{e}_x)$ and to the $(\mathbf{e}_z, \mathbf{e}_x)$ planes is presented

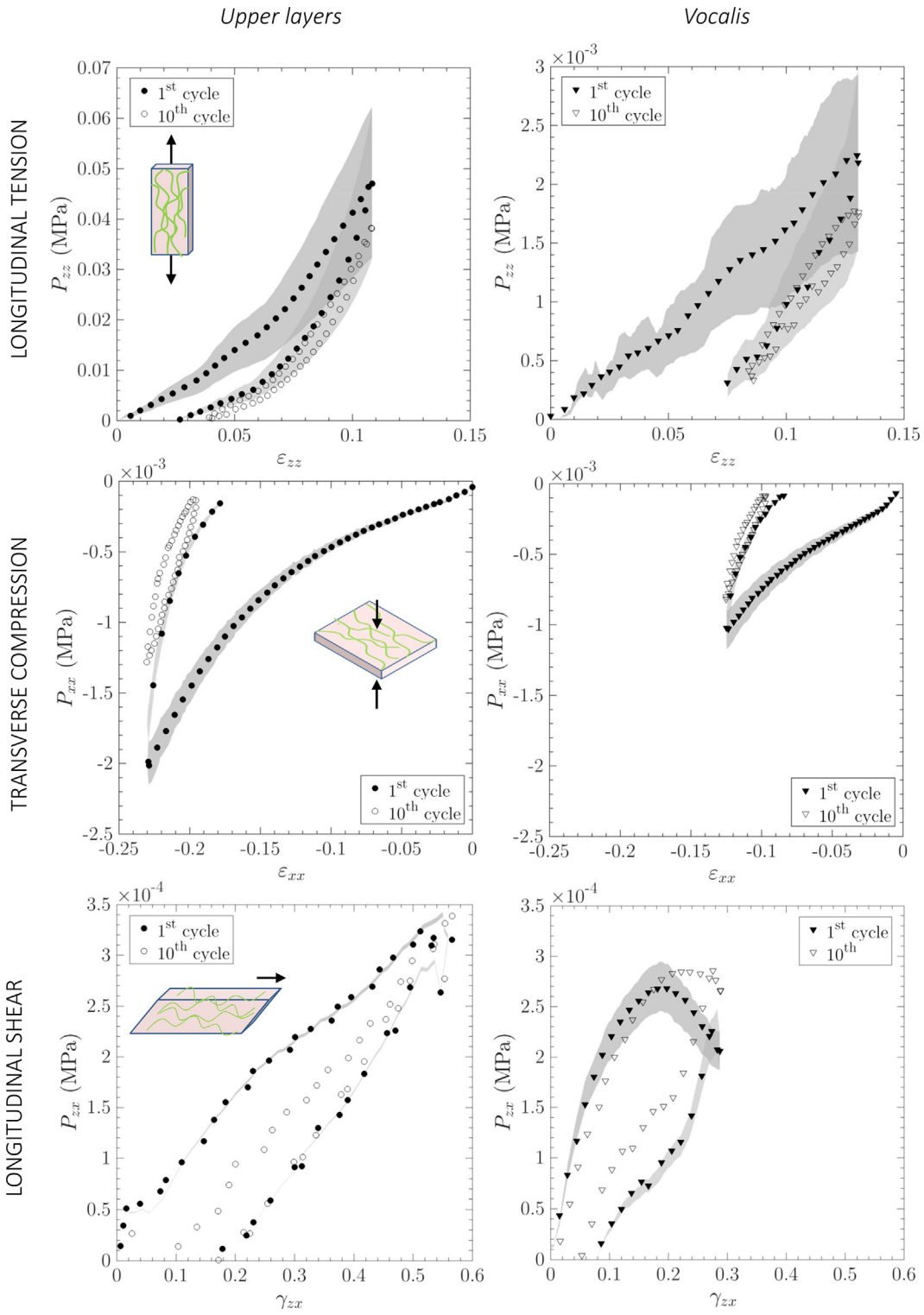

Fig. 4. Stress–strain curves in longitudinal tension, transverse compression and longitudinal shear (*from top to bottom*) of upper layers L_3–LP_2 (*left*) and vocalis L_3–M_2 (*right*). Gray corridors represent stress-data uncertainty (1st cycle only) induced by the estimation of the sample cross section S_0.

in Fig. 6(c). For both shear directions, the shape of the curve is similar but stresses are about twice higher in the $(\mathbf{e}_y, \mathbf{e}_x)$ plane, emphasising a marked anisotropy. This feature is confirmed in Fig. 6(d), displaying the anisotropic ratio G^t_{yx}/G^t_{zx} of the tangent shear moduli G^t_{yx} and G^t_{zx} with the shear strain for the 5 tested samples. Except for sample L_3-LP_1, the ratios G^t_{yx}/G^t_{zx} mainly range between 3 and 1 (mean value 1.55) and tend to decrease towards 1 ($G^t_{yx} \approx G^t_{zx}$). No clear difference was found between both sublayers.

4. Discussion and concluding remarks

This study provides original biomechanical data (20 samples) for excised human vocal folds, their upper layers and the *vocalis*,

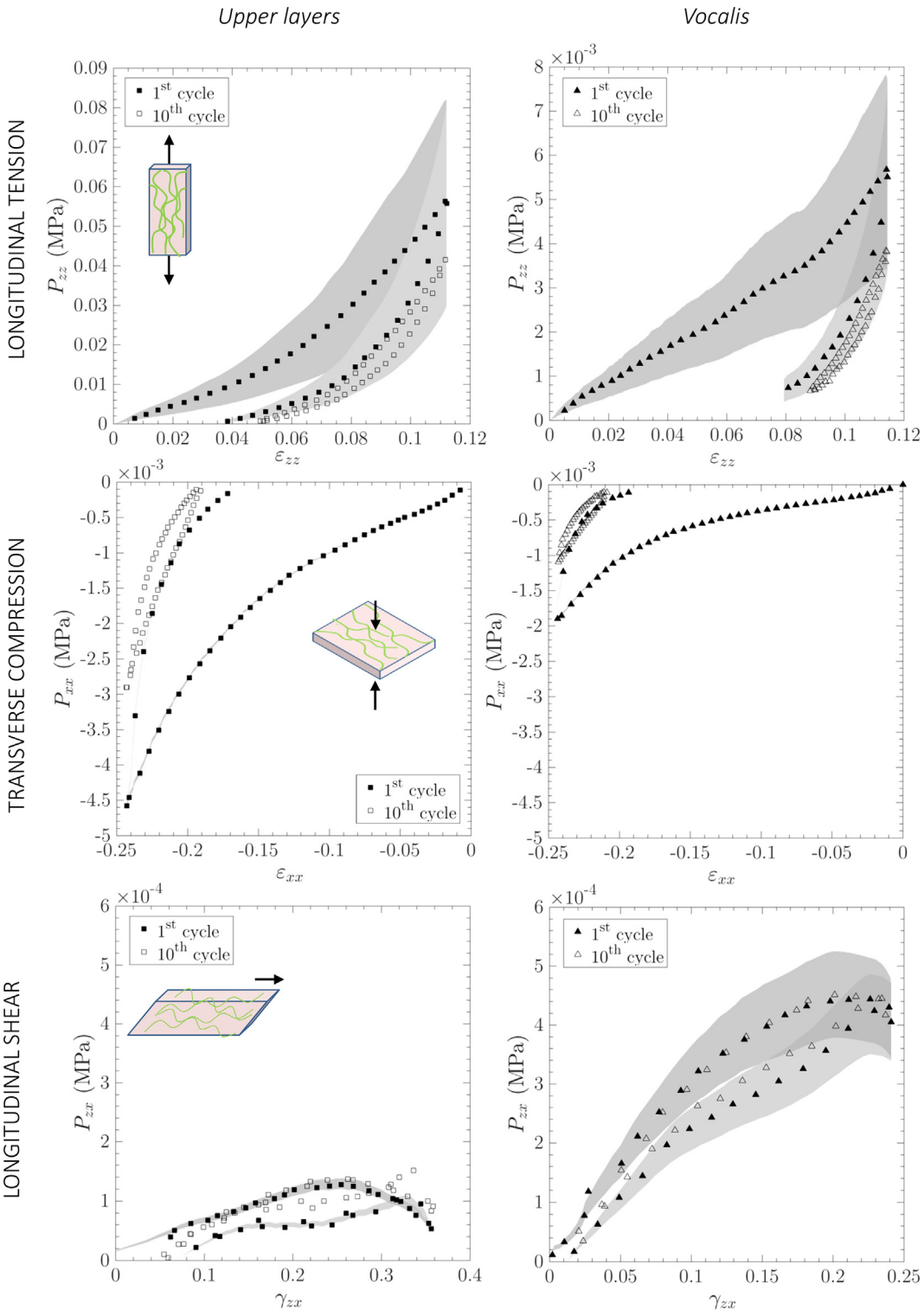

Fig. 5. Same as Fig. 4 for samples L_4–LP_2 (*left*) and L_4–M_2 (*right*).

by completing the knowledge of their finite strains mechanics in tension, compression and shear.

With respect to literature data, the database conjures up the following comments. In tension, the orders of magnitude of the longitudinal tangent modulus E_z^t of the upper layers are in agreement with previous *ex vivo* data. For instance, in the linear regime, Min et al. (1995) gave values around 20–50 kPa for the *lamina propria*. Other values range between 10 and 600 kPa for the isolated "cover" (*i.e., epithelium + lamina propria* superficial layer) (Chan et al., 2007; Kelleher et al., 2013; Kelleher et al., 2013b; Kelleher et al., 2011; Miri, 2014), and between 10 to 110 kPa for the "vocal ligament" (*i.e., lamina propria* mid and deep layers) (Chan et al., 2007; Kelleher et al., 2013; Kelleher et al., 2013b; Kelleher et al., 2011). For tensile strains above 0.4, the range is even wider, from 20 to 500 kPa for *lamina propria* (Min et al., 1995), up to 1850 kPa for cover (Chan et al., 2007) and 3300 kPa for ligament. The sources

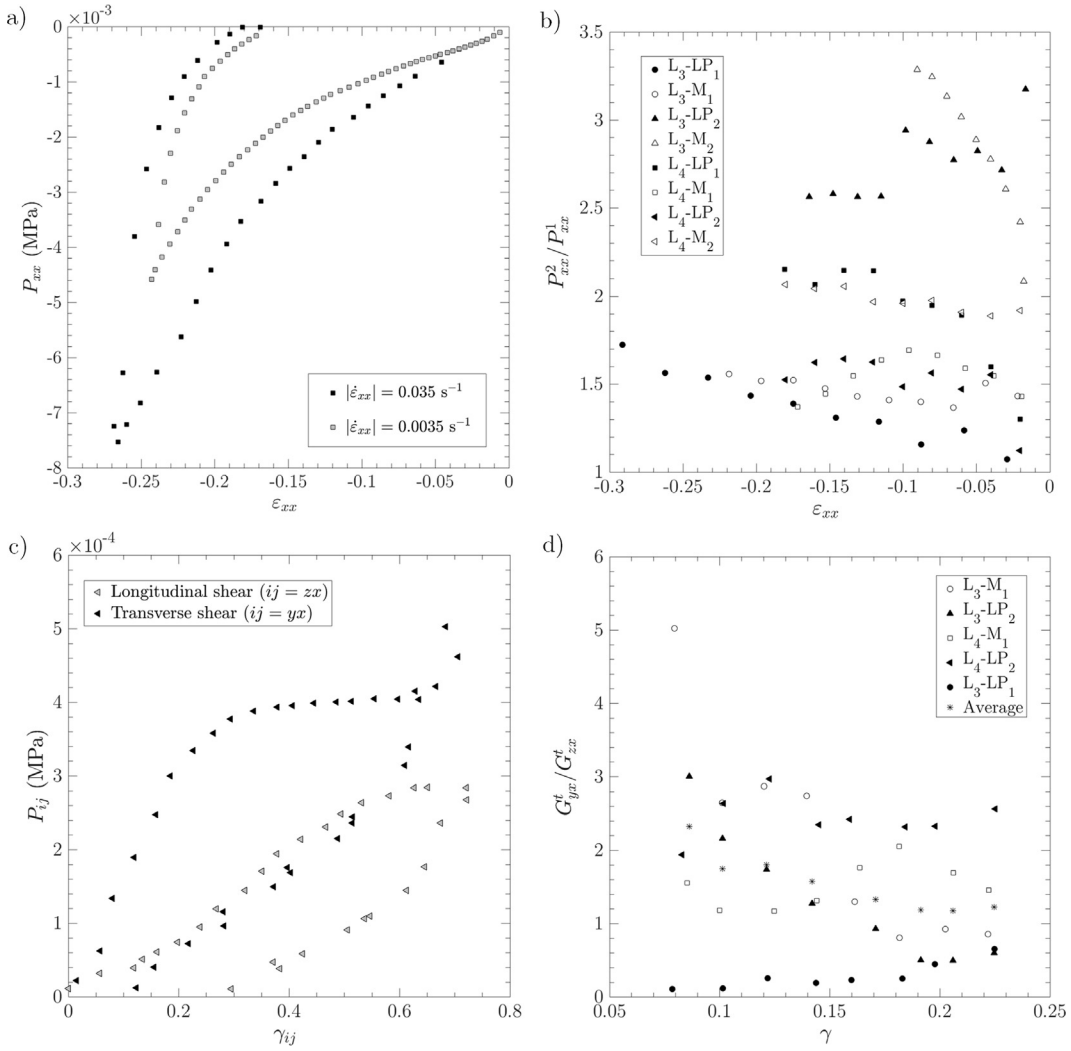

Fig. 6. (a) Compression stress–strain curves of sample L_4–LP_2 at two different initial strain rates $\dot{\varepsilon}_{xx}$; (b) Ratio of the compression stresses P^2_{xx}/P^1_{xx} as a function of the compression strain, for all tested samples; (c) Shear stress–strain curves of sample L_3–LP_1 deformed along the ($\mathbf{e}_z$, $\mathbf{e}_x$) and the ($\mathbf{e}_y$, $\mathbf{e}_x$) planes; (d) Anisotropic ratio G^t_{yx}/G^t_{zx} as a function of the shear strain.

of such a scattering are mainly related to intra/inter-individual variability. This was here again emphasised and conducted us to design a procedure to better compare experimental results (tension, compression and shear). In addition, to our knowledge, tensile data recorded for the human *vocalis* are original and cannot be compared with other literature data. Alternatively, close stress levels can be found on other skeletal muscles stretched along the main fiber direction such as *Longissimus dorsi* samples (10 kPa stress at a strain of 0.1), albeit taken from fresh pig tissues (Takaza et al., 2013). Furthermore, our shear data showed that the tangent shear moduli of the upper layers range from 0.36 to 2.3 kPa and from 0.25 to 2.5 kPa in the longitudinal and transverse direction, respectively. These values are similar to those obtained while shearing vocal-fold covers (without specifying the shearing plane), *i.e.,* between 1 Pa and 1 kPa (Chan and Rodriguez, 2008). Our estimates are also consistent with apparent elastic properties recorded with a linear skin rheometer (LSR) with vocal fold and sublayer samples (Rohlfs et al., 2013). In this study, the anisotropy of the apparent shear moduli was emphasised but the shear anisotropy ratio remained below 1 (0.5–0.75) at small apparent strains, whereas ours are such that $1 < G^t_{yx}/G^t_{zx} < 3$ within a larger strain range. Any further comparison is limited by uncertainties related to the assumptions stated both for the sample dimensions and the stress–strain state homogeneity using the LSR technique. Lastly, although transverse compression is a key mechanical loading during voice production (Tao and Jiang, 2007; Miri, 2014; Vampola and Horáček, 2014), compression experiments on vocal folds have not been reported so far. Few other biological materials have been characterised in compression, this loading being usually preferred for very soft tissues, the shear or tensile behaviour of which are tricky to characterise (Miller, 2005; Morriss et al., 2008). For instance, results can be found on adipose porcine tissue (Comley and Fleck, 2012), lung tissue (Andrikakou et al., 2016) or muscles (Pietsch et al., 2014; Böl et al., 2014): they emphasise non-linear properties similar to the trends highlighted here.

The present database shows that vocal-fold layers behave as many other soft living tissues subjected to finite strains, *i.e.,* with a non-linear viscoelastic and anisotropic behaviour exhibiting strain hardening and strain rate sensitivity, stress hysteresis and accommodation. These features are connected both to their inner gel-like ground substances and their orientated fibrous architectures which reorient, rearrange and deform differently with the loading mode and direction. In addition, by minimising the inter or intra-individual variability, the proposed experimental procedure allowed a quantitative comparison of results. Thus, important differences are emphasised for the aforementioned mechanical

features as a function of the loading modes. The mechanical role of the sublayers on the vocal folds mechanics is also better established. For instance, our data prove that the passive mechanical behaviour of the *vocalis* in tension is minor with respect to that of the upper layers. By contrast, stress levels achieved in compression and shear are close for both the upper layers and the *vocalis*. In addition, it is interesting to note that stress levels obtained in compression and shear are much (resp. moderately) lower than those obtained in tension for the upper layers (resp. the *vocalis*). Hence, by completing the existing database, these results constitutes a quantitative information for the validation of biomechanical models of phonation. It should also be completed, *e.g.,* by further scrutinising the strain rate sensitivity at higher strain rates, the accommodation and damage mechanisms, the link between the sublayer mechanics and the evolution of their inner fibrous architecture, and the active mechanics of the *vocalis*.

Declaration of Competing Interest

The authors declare no conflict of interest.

Acknowledgements

This work was supported by the LabEx Tec 21 (Investissements d'Avenir - grant agreement n° ANR-11-LABX-0030), the INSIS PEPS 2016 Micropli (CNRS) and the ANR MicroVoice n° ANR-17-CE19-0015–01. We would like to thank Philippe Masson, Alberto Terzolo, Anne McLeer-Florin and Philippe Chaffanjon for their helpful assistance.

Appendix A. Supplementary material

Supplementary data associated with this article can be found, in the online version, at https://doi.org/10.1016/j.jbiomech.2020.109956.

References

Andrikakou, P., Vickraman, K., and Arora, H. On the behaviour of lung tissue under tension and compression. Scientific Reports, 6 (1), 2016. doi:10.1038/srep36642. ISSN 2045-2322.

Bailly, L., Cochereau, T., Orgéas, L., Henrich Bernardoni, N., Rolland du Roscoat, S., McLeer-Florin, A., Robert, Y., Laval, X., Laurencin, T., Chaffanjon, P., Fayard, B., and Boller, E. 3d multiscale imaging of human vocal folds using synchrotron X-ray microtomography in phase retrieval mode. Scientific Reports, 8 (1): 14003, 2018. doi:10.1038/s41598-018-31849-w. ISSN 2045-2322.

Böl, M., Ehret, A.E., Leichsenring, K., Weichert, C., Kruse, R., 2014. On the anisotropy of skeletal muscle tissue under compression. Acta Biomater. 10 (7), 3225–3234. https://doi.org/10.1016/j.actbio.2014.03.003. ISSN 17427061.

Cavinato, C., Molimard, N.J. abd Curt, Campisi, S., Orgéas, L., and Badel, P. Does the knowledge of the local thickness of human ascending thoracic aneurysm walls improve their mechanical analysis? Frontiers in Bioengineering and Biotechnology, 7 (169): 1–12, 2019.

Chan, R.W., 2018. Nonlinear viscoelastic characterization of human vocal fold tissues under largeamplitude oscillatory shear (laos). J. Rheol. 62 (3), 695–712.

Chan, R.W. and Rodriguez, M.L.A simple-shear rheometer for linear viscoelastic characterization of vocal fold tissues at phonatory frequencies. The Journal of the Acoustical Society of America, 124 (2): 1207–1219, 2008. doi:10.1121/1.2946715. ISSN 0001-4966.

Chan, R.W., Titze, I.R., 1999. Viscoelastic shear properties of human vocal fold mucosa: measurement methodology and empirical results. J. Acoust. Soc. Am. 106 (4), 2008–2021.

Chan, R.W., Titze, I.R., 2003. Effect of postmortem changes and freezing on the viscoelastic properties of vocal fold tissues. Ann. Biomed. Eng. 31 (4), 482–491. https://doi.org/10.1114/1.1561287. ISSN 0090-6964.

Chan, R.W., Fu, M., Young, L., and Tirunagari, N. Relative Contributions of Collagen and Elastin to Elasticity of the Vocal Fold Under Tension. Annals of Biomedical Engineering, 35 (8): 1471–1483, 2007. 1573–9686. doi:10.1007/s10439-007-9314-x. http://link.springer.com/10.1007/s10439-007-9314-x. ISSN 0090-6964.

Comley, K., Fleck, N., 2012. The compressive response of porcine adipose tissue from low to high strain rate. Int. J. Impact Eng. 46, 1–10. https://doi.org/10.1016/j.ijimpeng.2011.12.009. ISSN 0734743X.

Dion, G.R., Jeswani, S., Roof, S., Fritz, M., Coelho, P.G., Sobieraj, M., Amin, M.R., and Branski, R.C. Functional assessment of the ex vivo vocal folds through biomechanical testing: A review. Materials Science and Engineering C, 64 (April): 444–453, 2016. ISSN 09284931.

Fratzl, P., Misof, K., Zizak, I., Rapp, G., Amenitsch, H., Bernstorff, S., 1998. Fibrillar Structure and Mechanical Properties of Collagen. J. Struct. Biol. 122 (1), 119–122. https://doi.org/10.1006/jsbi.1998.3966. ISSN 1047-8477.

Gasser, T.C., Ogden, R.W., and Holzapfel, G.A. Hyperelastic modelling of arterial layers with distributed collagen fibre orientations. Journal of The Royal Society Interface, 3 (6): 15–35, 2006. 1742–5662. doi:10.1098/rsif.2005.0073. ISSN 1742-5689.

Goodyer, E., Muller, F., Bramer, B., Chauhan, D., and Hess, M. In vivo measurement of the elastic properties of the human vocal fold. European Archives of Oto-Rhino-Laryngology, 263 (5): 455–462, 2006. 1434–4726. doi:10.1007/s00405-005-1034-y. ISSN 0937-4477.

Goodyer, E., Jiang, J.J., Devine, E.E., Sutor, A., Rupitsch, S., Zörner, S., Sting, M., and Schmidt, B. Devices and Methods on Analysis of Biomechanical Properties of Laryngeal Tissue and Substitute Materials. Current Bioinformatics, 6: 344–361, 2011. ISSN 15748936.

Gunter, H.E.A mechanical model of vocal-fold collision with high spatial and temporal resolution. The Journal of the Acoustical Society of America, 113 (2): 994–1000, 2003. doi:10.1121/1.1534100. ISSN 0001-4966.

Gunter, H.E., 2004. Modeling mechanical stresses as a factor in the etiology of benign vocal fold lesions. J. Biomech. 37 (7), 1119–1124. https://doi.org/10.1016/j.jbiomech.2003.11.007. ISSN 00219290.

Hantzakos, A., Remacle, M., Dikkers, F.G., Degols, J.-C., Delos, M., Friedrich, G., Giovanni, A., and Rasmussen, N. Exudative lesions of Reinke's space: a terminology proposal. European Archives of Oto-Rhino-Laryngology, 266 (6): 869–878, 2009. 1434–4726. doi:10.1007/s00405-008-0863-x. ISSN 0937-4477.

Hirano, M. Morphological Structure of the Vocal Cord as a Vibrator and its Variations. Folia Phoniatrica et Logopaedica, 26 (2): 89–94, 1974. 1421–9972. doi:10.1159/000263771. ISSN 1021-7762.

Isaksson, P., Dumont, P., and Rolland du Roscoat, S. Crack growth in planar elastic fiber materials. International Journal of Solids and Structures, 49 (13): 1900–1907, 2012. doi:10.1016/j.ijsolstr.2012.03.037. ISSN 00207683.

Kelleher, J., Zhang, K., Siegmund, T., Chan, R., 2010. Spatially varying properties of the vocal ligament contribute to its eigenfrequency response. J. Mech. Behav. Biomed. Mater. 3 (8), 600–609. https://doi.org/10.1016/j.jmbbm.2010.07.009. ISSN 17516161.

Kelleher, J.E., Siegmund, T., Chan, R.W., Henslee, E.A., 2011. Optical measurements of vocal fold tensile properties: Implications for phonatory mechanics. J. Biomech. 44 (9), 1729–1734. https://doi.org/10.1016/j.jbiomech.2011.03.037. ISSN 00219290.

Kelleher, J.E., Siegmund, T., Du, M., Naseri, E., Chan, R.W., 2013. The anisotropic hyperelastic biomechanical response of the vocal ligament and implications for frequency regulation: A case study. J. Acoust. Soc. Am. 133 (3), 1625–1636. https://doi.org/10.1121/1.4776204. ISSN 0001-4966.

Kelleher, J.E., Siegmund, T., Du, M., Naseri, E., Chan, R.W., 2013b. Empirical measurements of biomechanical anisotropy of the human vocal fold lamina propria. Biomech. Model. Mechanobiol. 12 (3), 555–567. https://doi.org/10.1007/s10237-012-0425-4.

Krasnoshlyk, V., Rolland du Roscoat, S., Dumont, P.J.J., Isaksson, P., Ando, E., Bonnin, A., 2018. Three-dimensional visualization and quantification of the fracture mechanisms in sparse fibre networks using multiscale X-ray microtomography. Proc. Roy. Soc. A: Math., Phys. Eng. Sci.

Lagier, A., 2016. Approche expérimentale de la collision entre les plis vocaux en phonation et du phonotraumatisme: Études in vivo et sur larynx humains excisés PhD Thesis. Aix-Marseille Univ.

Latil, P., Orgéas, L., Geindreau, C., Dumont, P., and Rolland du Roscoat, S. Towards the 3d in situ characterisation of deformation micro-mechanisms within a compressed bundle of fibres. Composites Science and Technology, 71 (4): 480–488, 2011. doi:10.1016/j.compscitech.2010.12.023. ISSN 02663538.

Laurencin, T., Orgéas, L., Dumont, P., Rolland du Roscoat, S., Laure, P., Le Corre, S., Silva, L., Mokso, R., and Terrien, M. 3d real-time and in situ characterisation of fibre kinematics in dilute non-Newtonian fibre suspensions during confined and lubricated compression flow. Composites Science and Technology, 134: 258–266, 2016. doi:10.1016/j.compscitech.2016.09.004. ISSN 02663538.

Miller, K., 2005. Method of testing very soft biological tissues in compression. J. Biomech. 38 (1), 153–158. https://doi.org/10.1016/j.jbiomech.2004.03.004. ISSN 00219290.

Min, Y.B., Titze, I.R., Alipour-Haghighi, F., 1995. Stress-strain response of the human vocal ligament. Ann. Otol. Rhinol. Laryngol. 104 (7), 563–569. https://doi.org/10.1177/000348949510400711. ISSN 0003-4894.

Miri, A.K., 2014. Mechanical Characterization of Vocal Fold Tissue: A Review Study. J. Voice 28 (6), 657–667. https://doi.org/10.1016/j.jvoice.2014.03.001. ISSN 08921997.

Miri, A.K., Heris, H.K., Tripathy, U., Wiseman, P.W., Mongeau, L., 2013. Microstructural characterization of vocal folds toward a strain-energy model of collagen remodeling. Acta Biomater. 9 (8), 7957–7967. https://doi.org/10.1016/j.actbio.2013.04.044. ISSN 17427061.

Morriss, L., Wittek, A., Miller, K., 2008. Compression testing of very soft biological tissues using semi-confined configuration: a word of caution. J. Biomech. 41 (1), 235–238. https://doi.org/10.1016/j.jbiomech.2007.06.025. ISSN 00219290.

Nicolle, S., Palierne, J.-F., 2010. Dehydration effect on the mechanical behaviour of biological soft tissues: Observations on kidney tissues. J. Mech. Behav. Biomed. Mater. 3, 630–635.

Pietsch, R., Wheatley, B.B., Haut Donahue, T.L., Gilbrech, R., Prabhu, R., Liao, J., and Williams, L.N. Anisotropic Compressive Properties of Passive Porcine Muscle

Tissue. Journal of Biomechanical Engineering, 136 (11): 111003–8, 2014. doi:10.1115/1.4028088. ISSN 0148-0731.

Remache, D., Caliez, M., Gratton, M., Dos Santos, S., 2018. The effects of cyclic tensile and stress-relaxation tests on porcine skin. J. Mech. Behav. Biomed. Mater. 77, 242–249.

Rohlfs, A.-K., Goodyer, E., Clauditz, T., Hess, M., Kob, M., Koops, S., Püschel, K., Roemer, F.W., and Müller, F. The anisotropic nature of the human vocal fold: an ex vivo study. European Archives of Oto-Rhino-Laryngology, 270 (6): 1885–1895, 2013. 1434–4726. doi:10.1007/s00405-013-2428-x. ISSN 0937-4477.

Takaza, M., Moerman, K.M., Gindre, J., Lyons, G., Simms, C.K., 2013. The anisotropic mechanical behaviour of passive skeletal muscle tissue subjected to large tensile strain. J. Mech. Behav. Biomed. Mater. 17, 209–220.

Tao, C., Jiang, J.J., 2007. Mechanical stress during phonation in a self-oscillating finite-element vocal fold model. J. Biomech. 40 (10), 2191–2198. https://doi.org/10.1016/j.jbiomech.2006.10.030. ISSN 00219290.

Vampola, T. and Horáček, J. Simulation of vibration of the human vocal folds. In Proceedings of the 9th International Conference on Structural Dynamics, EURODYN 2014, 2014.

Vampola, T., Horáček, J., Klepáček, I., 2016. Computer simulation of mucosal waves on vibrating human vocal folds. Biocybernet. Biomed. Eng. 36 (3), 451–465. https://doi.org/10.1016/j.bbe.2016.03.004. ISSN 02085216.

Zhang, K., Siegmund, T., Chan, R.W., 2009. Modeling of the transient responses of the vocal fold lamina propria. J. Mech. Behav. Biomed. Mater. 2 (1), 93–104. https://doi.org/10.1016/j.jmbbm.2008.05.005. ISSN 17516161.